ARCHIVES OF ELECTRICAL ENGINEERING VOL. 68(4), pp. 933–946 (2019)

DOI 10.24425/aee.2019.130693

An analysis of a start-up process in LSPMSMs with aluminum and copper rotor bars considering the coupling of electromagnetic and thermal phenomena

MARIUSZ BARANSKI, WOJCIECH SZELAG, WIESLAW LYSKAWINSKI

Institute of Electrical Engineering and Electronics
Poznan University of Technology
Piotrowo 3A str., 60-965 Poznan, Poland
e-mails: {mariusz.baranski/wojciech.szelag/wieslaw.lyskawinski}@put.poznan.pl

(Received: 17.05.2019, revised: 18.08.2019)

Abstract: The paper presents an FE model of coupled electromagnetic and thermal phenomena in Line Start Permanent Magnet Synchronous Motors (LSPMSMs). An algorithm for solving equations of a discrete model using the FEM has been presented. On the basis of this algorithm the author's personally developed software for the analysis of coupled electromagnetic-thermal phenomena in the LSPMS motors was elaborated. This software was used to analyze the start-up process of motors with identical stator and rotor magnetic circuits and different materials of the starting cage. The start-up process of motors with the squirrel-cage made of aluminum and copper was considered. The influence of temperature on the start-up process has been taken into account. The results of simulation tests were compared with the results of measurements.

Key words: aluminum and copper cage, coupled electromagnetic-thermal phenomena, FE model of LSPMSM, measurement verification, start-up process

1. Introduction

In the pursuit to reduce electricity consumption, permanent magnet synchronous motors (PMSMs) are increasingly used in electric drives. The permanent magnet motors exhibit a power factor of near unity and a high efficiency. The greatest financial and ecological benefits associated with the use of these types of PMSMs will be achieved due to their widespread use, especially in continuous running drives. The permanent magnet motors are used in both electric drives operating at constant and regulated speed. These two types of motors differ in the design and

method of power supply. The motors designed for operation at variable speed are supplied from power electronic systems. Drives of these types are expensive and more unreliable due to the use of power electronic converters. However, the motors designed for constant speed operation are adapted for line start-up and are supplied directly from the power grid. The lack of power electronics systems reduces the price and increases the reliability of the drives. The asynchronous moment generated by the cage winding placed in the rotor is used to start the LSPMSMs. The disadvantage of the asynchronous start-up is the high value of the inrush current in the stator winding that arises directly after connecting the motor to the supply network. The value of the starting current can be up to 4 to 10 times the nominal current. For this reason, a starting process by direct connection to the grid is most often used in small and medium power motors. Moreover, when designing such a type of motor, on top of meeting the requirements for parameters for steady-state operation, additional requirements related to asynchronous operation, regarding minimum starting torque, stalling torque and falling into synchronism state must be realized [1–3]. Due to a high power factor and very high efficiency and operational reliability, the LSPMSM are increasingly used in many industries applying high energy-saving drives, e.g. in mining [4].

For the above reasons, many scientific and research centers [5–11], carry-out intensive work on these types of motors [12, 13].

The disadvantage of the LSPMSM is the possibility of partial demagnetization of the magnets by a high armature reaction field accompanying the starting process and thermal sensitivity of the permanent magnets. The armature reaction field occurs, among others, when starting a motor. The starting current depends on the supply voltage, the value of back electromotive force, the impedance of the windings and the construction of the motor. In addition, a very large effect on the current and motor speed time curves during the start-up process is shaped by the mechanical characteristics and moment of inertia of the load. The start-up time depends on the dynamic torque, i.e. the surplus of the electromagnetic torque over the anti-torque, and it increases with the moment of inertia. With the increase of the starting current and the start-up time, the power losses in the stator and rotor windings increase, and thus also the temperature of the motor components. Due to the above reasons, particularly dangerous for the motor in terms of heat are frequently repeated starting processes occurring at a low dynamic moment and high load inertia moment. The fans are an example of this type of load. The temperature increments in the motor during frequently repeated starting processes are cumulative. As a result, after the next starting process of the motor, the temperature may be higher than the temperature obtained in the thermal steady state of the motor operating at rated load conditions.

On the other hand, the increase in the temperature of magnets reduces the resistance of magnets to partial demagnetization [14]. As a result of the partial demagnetization of the magnets, the magnetic flux in the machine is reduced and in consequence the main operating parameters of the machine deteriorate. The paper attempts to improve the LSPMSM starting parameters. For this purpose, the influence of the type of material from which the rotor cage windings were made over the course of the LSPMSM start-up process was analyzed. The starting process of the motor with the same magnetic circuit shape but with a cage winding made of aluminum or copper was considered. As is well known from the literature, the resistivity of the material from which the cage winding was made of affects both the process of starting the motor and the process of falling into synchronism [14–16]. The influence of temperature on the change of thermal properties of materials, electrical properties of conductive materials, and magnetic properties of permanent

magnets has been taken into account. The analysis was carried out taking into account the dynamic impact of the starting inrush current on the state of magnetization of permanent magnets. Due to the coupling of electromagnetic and thermal phenomena and their relation to the rotational motion of the rotor, a field model of the LSPMSM was used to describe the working of the machine. The algorithm for solving equations of a discrete model as well as author's personally developed on its basis software for analyzing coupled electromagnetic and thermal phenomena in the considered LSPMSM are discussed in Section 2.

2. Mathematical model of LSPMSM

The distribution of a low frequency transient electromagnetic field in the studied motor can be determined by:

$$\operatorname{rot}(\nu \operatorname{rot} \boldsymbol{A}) = \boldsymbol{J} + \boldsymbol{J}_m, \tag{1}$$

where $\boldsymbol{J}_m = \operatorname{rot} \boldsymbol{H}_m$ is the current density vector representing the magnetization of the permanent magnet, $\boldsymbol{J} = \gamma \left(\operatorname{grad} V_e - \dfrac{\partial \boldsymbol{A}}{\partial t} \right)$ is the current density vector, $\boldsymbol{H}_m$ is the magnetization vector in the region with permanent magnets, ν is the magnetic reluctivity, γ is the conductivity of the medium, $\boldsymbol{A}$ is the magnetic vector potential, V_e is the scalar electric potential. In the considerations, it was assumed that the electromagnetic field in the motor is two-dimensional and characterized by axial symmetry.

It has been taken into account that the magnetic properties of the core and the permanent magnets are described by Equations (2) and (3), respectively.

$$\boldsymbol{H} = \nu \boldsymbol{B} \tag{2}$$

and

$$\boldsymbol{B} = \mu_0 (\boldsymbol{H} + \boldsymbol{H}_m), \tag{3}$$

where $\boldsymbol{B}$ is the vector of magnetic flux density, $\boldsymbol{H}$ is the magnetic field strength vector, μ_0 is the magnetic permeability of the vacuum.

The loop equations of the electric circuit as well as the winding of the motor can be introduced to the following model:

$$\boldsymbol{u} = \boldsymbol{R}\boldsymbol{i} + \boldsymbol{L}\frac{\mathrm{d}}{\mathrm{d}t}\boldsymbol{i} + \frac{\mathrm{d}}{\mathrm{d}t}\boldsymbol{\Psi}, \tag{4}$$

where $\boldsymbol{u}$ is the vector of supply voltages, $\boldsymbol{R}$ is the matrix of loop resistances, $\boldsymbol{i}$ is the vector of loop currents, $\boldsymbol{\Psi}$ is the flux linkage vector calculated by means of the field model.

In the field model of the LSPMSM presented above, equations are coupled with the mechanical equilibrium equation of the drive system [17, 18] through the electromagnetic torque T.

$$J_i \frac{\mathrm{d}^2 \beta}{\mathrm{d}t^2} + T_L = T, \tag{5}$$

where J_i is the moment of inertia of the movable elements of the system, β is the angular position of the rotor, T_L is the load torque. The driving torque T is determined on the basis of the calculated magnetic field distribution [18].

During the processing of the electric energy in the motor, stator winding and core losses are generated. These losses cause the motor to heat up. The temperature change of the motor components affects the course of electromagnetic phenomena by changing the electrical properties of conductive materials and the magnetic properties of permanent magnets. In addition, the temperature also affects the change in thermal properties of the materials [14, 17, 19]. For this reason it is necessary to take into account a heat transfer equation in the electromagnetic model of the LSPMSM [17, 20].

$$\operatorname{div}(\lambda \operatorname{grad} \tau) + p_h = c_h \rho \frac{\mathrm{d}\tau}{\mathrm{d}t}, \tag{6}$$

where p_h is the power loss density, τ is the temperature, λ is the tensor of thermal conductivity, ρ is the specific mass, c_h is the specific heat.

The first component on the left side of the equation represents heat conduction, and the component on the right side shows local temperature changes over time.

It has been assumed that the power loss density in the core is determined in a simplified way on the basis of the magnetic field distribution in the machine core and the specific total loss in W/kg of electrical steels [17, 21]. The thermal flux q_n that penetrates the external surface of the motor is proportional to the temperature difference between this surface and the surroundings

$$q_n = \lambda \frac{\partial \tau}{\partial n} = -\kappa(\tau_S - \tau_A), \tag{7}$$

where τ_A is the ambient temperature, τ_S is the bulk temperature of the fluid, and κ is the heat transfer coefficient.

As is well known, both conductive and convective heat transfers occur in the air gap between the rotor and the stator of rotating electrical machines. Therefore, the effective thermal conductivity which captures both conduction and convection in the air gap must be determined. In this paper the convective heat coefficients are calculated considering the state of the air flow in the air gap [19]. For the purpose of calculating the temperature in the outer surface of the frame of the motor cooled with an air stream, a corrected heat transfer coefficient in (7) was expressed according to the following relationship:

$$\kappa = \kappa_n \left(1 + w_v \sqrt{v}\right), \tag{8}$$

where κ_n is the natural thermal conductivity coefficient, v is the linear velocity mover, w_v is the coefficient characterized by the cooling intensity.

In order to solve non-linear Equations (1)–(7) describing a coupled electromagnetic and thermal field in the LSPMSM, only approximate methods can be applied, based on the discretization of space and time. The FEM was used to determine the magnetic field and thermal field distributions in the motor. For this purpose, the considered domain has been subdivided into triangular elements. After the discretization of the time by use of a backward difference scheme, Equations (1)–(7) can be expressed in the form of a system of algebraic nonlinear equations

$$\begin{bmatrix} \boldsymbol{S}^n + \boldsymbol{G}(\mathbf{1} - \boldsymbol{M})\Delta t^{-1} & \boldsymbol{N} \\ -\boldsymbol{N}^T & -(\boldsymbol{R}\Delta t + \boldsymbol{L}) \end{bmatrix} \begin{bmatrix} \boldsymbol{\varphi}^n \\ \boldsymbol{i}^n \end{bmatrix} = \begin{bmatrix} \boldsymbol{\theta}_m^n \\ -\Delta t \boldsymbol{U}^n \end{bmatrix} + \begin{bmatrix} \boldsymbol{G}(\mathbf{1} - \boldsymbol{M})\Delta t^{-1} & \mathbf{0} \\ -\boldsymbol{N}^T & -\boldsymbol{L} \end{bmatrix} \begin{bmatrix} \boldsymbol{\varphi}^{n-1} \\ \boldsymbol{i}^{n-1} \end{bmatrix}, \tag{9}$$

$$\frac{J_i\left(\beta^{n+1}-2\beta^n+\beta^{n-1}\right)}{(\Delta t)^2}=T^n-T_L^n-T_f^n, \tag{10}$$

$$\left(\boldsymbol{S}_\tau^n+\boldsymbol{K}_{\tau b}^n+\boldsymbol{M}_\tau^n\Delta t^{-1}\right)\tau^n=\boldsymbol{P}^n+\boldsymbol{K}_{\tau o}^n+\boldsymbol{M}_\tau^n\Delta t^{-1}\tau^{n-1}, \tag{11}$$

where $\boldsymbol{S}$ is the magnetic reluctance matrix, $\boldsymbol{\varphi}$ is the vector of potential $\boldsymbol{\varphi}$ in nodes of the mesh, $\boldsymbol{i}$ is the vector of loop currents, $\boldsymbol{M}$ is the matrix of coefficients, $\boldsymbol{R}$ and $\boldsymbol{L}$ are the matrices of resistances and inductances of the windings and supply the system circuit, respectively, $\boldsymbol{N}$ is the matrix describing the number of turns assigned to the mesh nodes, $\boldsymbol{G}$ is the matrix of equivalent electrical conductances, $\boldsymbol{\theta}_m$ is the vector representing the magnetization of the permanent magnets, $\boldsymbol{S}_\tau$ is the matrix of thermal conductances, $\boldsymbol{M}_\tau$ is the matrix of thermal capacitances, τ is the vector of unknown temperatures, $\boldsymbol{P}$ is the vector of heat sources, $\boldsymbol{K}_{\tau b}$ and $\boldsymbol{K}_{\tau o}$ are the matrices of the coefficient describing heat transfer to the environment of the motor. $\Delta t = t_n - t_{n-1}$ is the time step length, n and $n-1$ denote the quantities of the current $t = t_n$, and the previous $t = t_{n-1}$ time-step number. For example: $\boldsymbol{S}^n = \boldsymbol{S}(t_n)$, $\boldsymbol{\varphi}^n = \boldsymbol{\varphi}(t_n)$.

The elements of the vector $\boldsymbol{\theta}_m$, matrices $\boldsymbol{R}$, $\boldsymbol{G}$ and $\boldsymbol{S}_\tau$, in the elaborated mathematical model of coupled phenomena of the LSPMSM, depend on temperature [14, 17, 19, 21]. The components of the magnetization vector $\boldsymbol{\theta}_m$ are calculated accordingly to families of demagnetization characteristics and interpolation techniques in relation to magnetic flux density, magnetic field intensity and temperature [14]. In the discretized model, the movement of the rotor is simulated by means of the distorted element. To solve the Equations (9)–(11) of the discretized model, the authors applied the block-over relaxation method. It was assumed that the calculation blocks correspond to the particular equations of the used discrete model of coupled phenomena. An advantage of the block-over relaxation method is the possibility of using the classic effective Newton–Raphson procedure for an independent iterative solution of non-linear Equations (9)–(11). On the basis of the presented algorithm for solving the 2D equations of the field model of coupled phenomena, the author's special software for analyzing a transient LSPMSM has been developed. The software has been developed in the Borland–Delphi environment.

3. Examined motor

Figure 1 shows the structure of the considered LSPMSM motor. The studied motor has been developed and built at the Division of Electrical Machines and Mechatronics of Poznan University of Technology. During the design process it has been assumed that geometry of the stator core is given in advance. The stator core shape of the mass-produced, general purpose, 3-phase, 4-pole, 3 kW output power squirrel cage motor of the Sg100L-4B type has been used. The rated torque of the squirrel cage motor is $T_N = 20$ Nm. Figure 1(b) illustrates directions of heat flow in the considered motor.

The analyzed motor has 36 drop-shaped slots in the stator and the squirrel cage of 28 bars in the rotor. Each rotor pole is formed by 3 NdFeB magnets of the N38SH type arranged in a "U" shape inside the rotor core. The motor is supplied by a 3-phase balanced system of 400 V line to line voltage and its phase windings are arranged into the star connection. The wire insulation temperature class is 155°C.

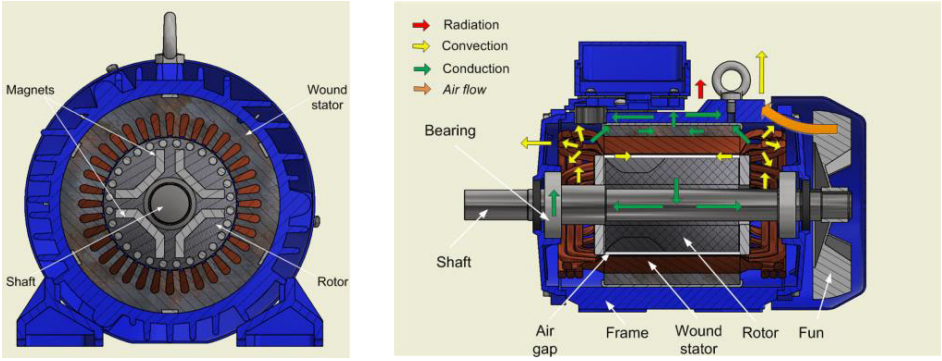

(a) (b)

Fig. 1. A cross-section (a) and a longitudinal section (b) of the LSPMSM motor – directions of thermal flows

4. Results

The author's software developed on the basis of the presented in Section 2 algorithm for solving equations of a discrete motor model, has been used to the analysis of the starting process of an LSPMSM presented in Section 3. In the discrete 2D model of the LSPMSM, the number of potentials φ and edge temperatures τ was around 37 000 and 40 000, respectively.

The results of the study on the reliability of the developed algorithm and software for the analysis of coupled electromagnetic and thermal phenomena are presented, among others, in works [14, 17]. These papers are limited to presenting the results of the process of selecting the parameters of the thermal model of the machine. The thermal model tuning was performed by selecting the κ heat release coefficient from the machine surface. It was aimed at the selection of the κ coefficient determined by Equation (8), for which the obtained results of the calculations show the best compatibility with the results of the experimental tests of the heating process.

Figure 2 shows the calculated and measured increase of the average temperature of the stator winding in the LSPMSM for both aluminum rotor bars and copper rotor bars. To measure the

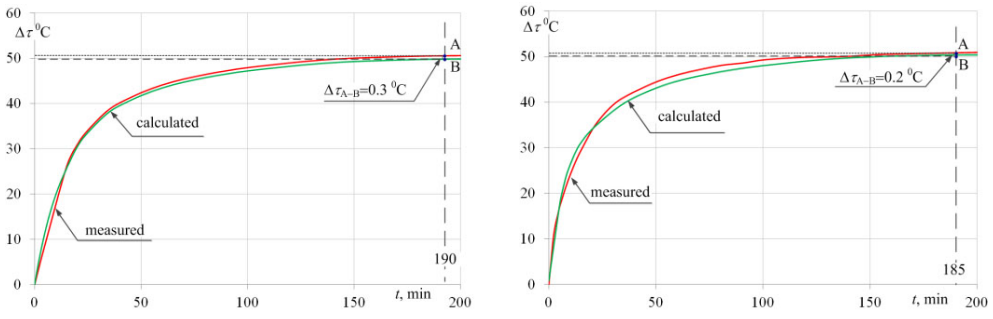

(a) (b)

Fig. 2. Calculated and measured increase of the average temperature of the stator winding: (a) aluminium bar; (b) copper bar for $U = 400$ V and $T_L = 24$ Nm

temperature of the coils belonging to different groups of phase windings, PT-100 temperature sensors were used. These sensors were arranged along the circumference of the stator core, halfway through the length of the slots in the area of the slot opening, next to the winding surface. The calculations were carried out until a thermally steady-state was obtained. It was assumed that the thermal steady-state is reached when the increase of temperature is not greater than 2°C per hour.

While testing the influence of a type of material from which the cage winding was made over the course of the LSPMSM start-up process, the temperature distribution τ_p $(t = 0, x, y)$ in the machine was taken into account when the time during the connection of the motor to the voltage $U = 400$ V was equal to 0 $(t = 0)$. The mechanical characteristic $T_L(n)$ of the device driven by the motor, used in the calculations, is shown in Figure 3. In order to shorten the description of the mechanical characteristics of the motor load, it was assumed that this characteristics is clearly defined by the load moment at a speed of $n = 1\,500$ rpm, i.e. $T_L = T_L\ (1\,500\ \text{rpm}) = 19.8$ Nm. It was also suggested that the moment of inertia of load J_i can vary within the range of 0.004 to 0.084 kg·m^2, where $J_i = 0.0083$ kg·m^2 is the value of the nominal moment of inertia of the rotor.

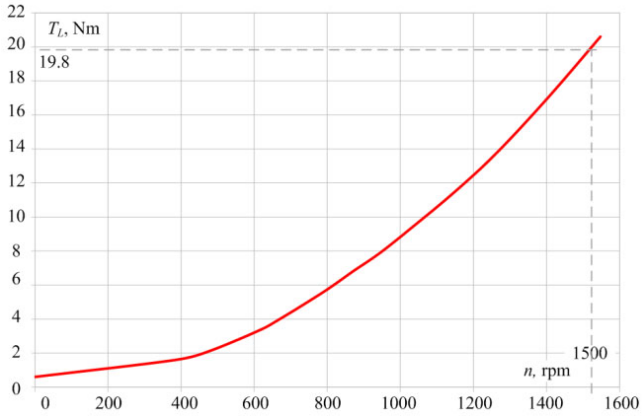

Fig. 3. Mechanical characteristic $T_L(n)$ of load

The calculations were carried out taking into account the influence of temperature on the resistivity of the materials from which the windings were made of, this influence on the magnetic properties of permanent magnets as well as on the thermal properties of the materials. The influence of the values J_i during the moment of inertia of the load and the influence of the distribution of the initial temperature τ_p $(t = 0, x, y)$ on the waveforms of the electromagnetic torque $T(t)$, the speed n(t) and the phase currents $i_a(t)$, $i_b(t)$, $i_c(t)$, have been studied. The simulation of the start-up processes was carried out for two given temperature distributions in the area of the machine at the moment of connection to the grid. First, it was assumed that during the start-up of the motor the temperature in the machine area has a constant value, i.e. $\tau_p(t = 0, x, y) = 20$°C. Then the start-up of the motor was analyzed assuming that the initial temperature distribution $\tau_p(t = 0, x, y)$ and the temperature distribution τ_u (t_u, x, y) in the motor during the electromagnetic and thermal steady-state condition are equal, wherein t_u denotes the time which elapsed from the start-up moment of the loaded motor $T_L = 19.8$ Nm to the moment when the motor obtained the thermal steady-state condition. The temperature distribution in the

steady-state after the start-up process of the motor is shown in Figure 4. When determining this distribution, it was assumed that before the motor was started, the temperature of all its components was constant and amounted to $\tau_p(t = 0, x, y) = 20°\text{C}$. There was no power loss in the rotor of the LSPMSM during the electromagnetic and thermal steady-state condition. For this reason, the temperature field distributions for motors with a rotor cage made of aluminum and copper are the same. This thermal distribution does not depend on the values J_i of the moment of inertia in movable elements of the system.

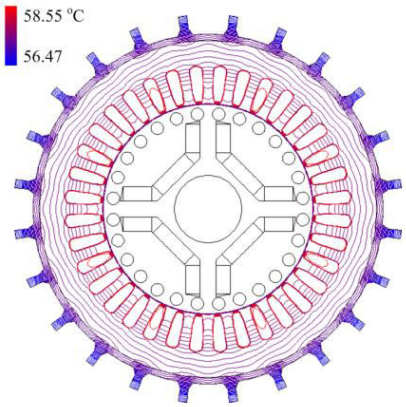

Fig. 4. Thermal field distribution $\tau_u\ (t_u, x, y)$ in electromagnetically and thermal steady-state condition for $T_L = 19.8$ Nm, $U = 400$ V, $\tau_p(t = 0, x, y) = 20°\text{C}$

The comparison of the selected time curves of the phase currents $i_a(t)$, the electromagnetic torque $T(t)$ and the speed of rotors $n(t)$ during the starting of the motor with the rotor cage made of aluminum (Al) and copper (Cu) is shown in Figure 5. These time curves were obtained assuming that $\tau_p(t = 0, x, y) = 20°\text{C}$, $T_L = 19.8$ Nm and $J_i = 0.012$ kg·m^2. However, the time curves $i_a(t)$, $T(t)$ and $n(t)$ during the start-up, carried out for $\tau_p(t = 0, x, y) = \tau_u(t_u, x, y)$ and for the same load torque and moment of inertia, are as shown in Figure 6.

Figures 5 and 6 show that the higher impact value of the inrush current in the stator winding and starting torque, as well as a shorter start-up time are obtained for the motor with copper cage bars. The starting process of the motor with the copper bars in the rotor is characterized by greater dynamics and certainty of falling into synchronism. The obtained results confirm that regardless of the type of the cage material, the increase in temperature makes it difficult to start-up the motor. This is mainly due to the reduction of the magnetic flux generated by permanent magnets along with the temperature rises.

On the other hand, the temperature field distributions in the motors after the above described start-up processes for time $t = 0.17$ s (electromagnetically steady-state) are shown in Figures 7(a–d), respectively. The results show that due to the short time of the considered start-up processes, the maximum temperature increase in the motor is small and does not exceed 0.50°C.

The influence of the values J_i during the moment of inertia of the load on the time curves of the starting process of motors with aluminum and copper cage rotor bars was also analyzed. The calculations were repeated for two initial temperature distributions in the machine, i.e. $\tau_p(t = 0, x, y) = 20°\text{C}$ and $\tau_p(t = 0, x, y) = \tau_u(t_u, x, y)$. It was assumed that the loaded moment was equal to $T_L = 19.8$ Nm. The rotor speed time curves obtained during starting of the motor are shown in Figure 8.

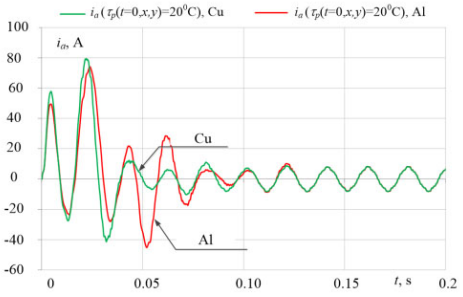

(a)

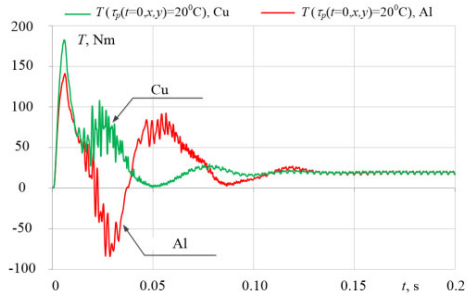

(b)

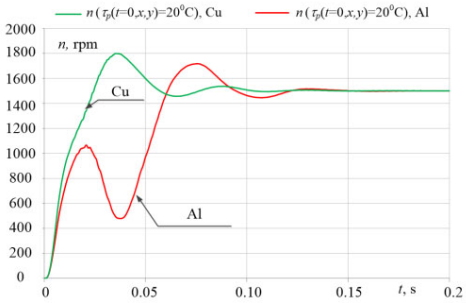

(c)

Fig. 5. Time curves of phase current (a); electromagnetic torque (b) and rotor speed (c) in motors with aluminum rotor bars (Al) and copper rotor bars (Cu) for $\tau_p(t = 0, x, y) = 20°C$, $T_L = 19.8$ Nm, $J_i = 0.012$ kg·m^2

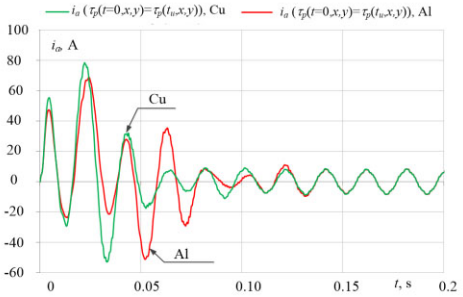

(a)

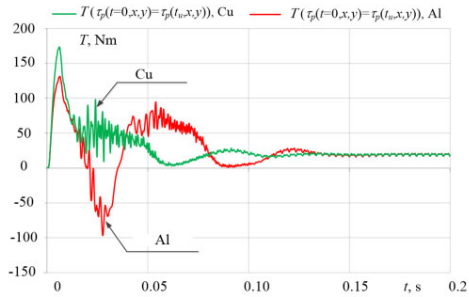

(b)

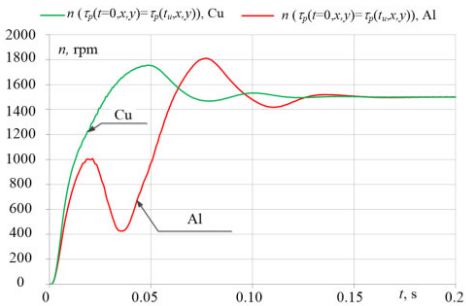

(c)

Fig. 6. Time curves of phase current (a); electromagnetic torque (b) and rotor speed (c) in motors with aluminum rotor bars (Al) and copper rotor bars (Cu) for $\tau_p(t = 0, x, y) = \tau_u(t_u, x, y)$, $T_L = 19.8$ Nm, $J_i = 0.012$ kg·m^2

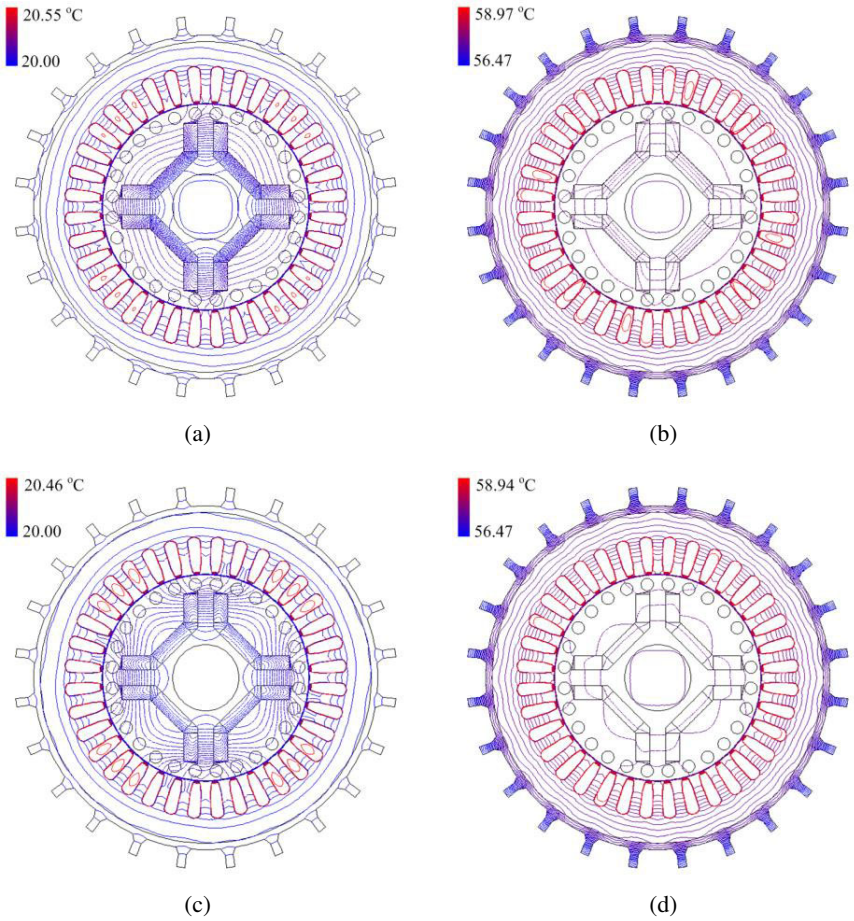

Fig. 7. Thermal field distribution for $t = 0.17$ s in motor with aluminum rotor bars for (a) $\tau_p(t = 0, x, y) = 20°\text{C}$; (b) $\tau_p(t = 0, x, y) = \tau_u(t_u, x, y)$ and in motor with copper rotor bars for (c) $\tau_p(t = 0, x, y) = 20°\text{C}$; (d) $\tau_p(t = 0, x, y) = \tau_u(t_u, x, y)$

On the basis of the presented results, it can be concluded that the material a cage winding is built of, has a very big influence on the speed time curve during a start-up process. The squirrel-cage rotor made of copper material enables the LSPMSM to be started with a much greater moment of inertia in movable elements of the system than the squirrel-cage rotor made of aluminum material. From the obtained time curves presented in Figure 8 it also follows that when the "cold" motor ($\tau_p(t = 0, x, y) = 20°\text{C}$) with the aluminum cage winding is started, the motor synchronizes correctly for $J_i \leq 0.052$ kg·m^2. During the start of the "warm" motor ($\tau_p(t = 0, x, y) = \tau_u(t_u, x, y)$) the rotor falls into synchronism when $J_i \leq 0.036$ kg·m^2. However, in order to obtain a proper start of "cold" and "warm" motors with the cage made of copper, the moment of inertia must meet the conditions $J_i \leq 0.0076$ kg·m^2 and $J_i \leq 0.084$ kg·m^2, respectively.

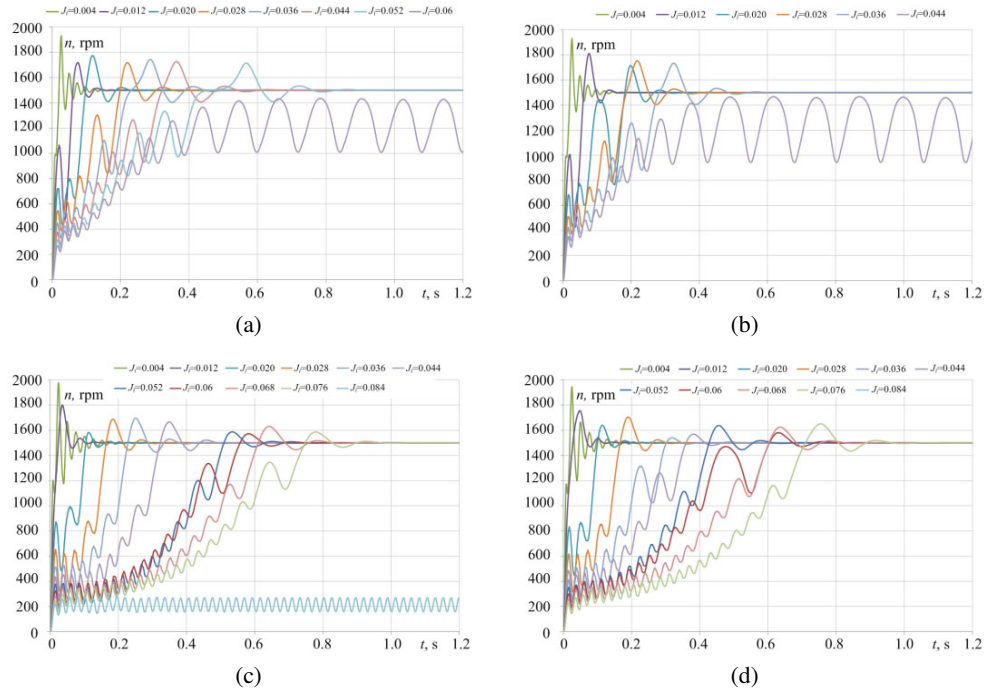

Fig. 8. Rotor speed time curve*n* of the motor with aluminum rotor bars for (a) $\tau_p(t = 0, x, y) = 20°C$; (b) $\tau_p(t = 0, x, y) = \tau_u(t_u, x, y)$ and in motor with copper rotor bars for (c) $\tau_p(t = 0, x, y) = 20°C$; (d) $\tau_p(t = 0, x, y) = \tau_u(t_u, x, y)$, $T_L = 19.8$ Nm, $J_i = \text{var}$

It can be concluded that given the same shape of the cage winding bars, the motor with the cage made of copper has a much better start-up parameters. It should be emphasized that after completing the calculations for each moment of inertia, it was checked whether the permanent excitation magnets in the machine were not partially demagnetized. The original author's algorithm presented in [14] was used for this purpose.

The comparison of the rotor speed time curves during the start-up process for the motors with copper and aluminum cage rotor bars when $J_i = 0.036$ kg·m^2, is shown in Figure 9. For this value

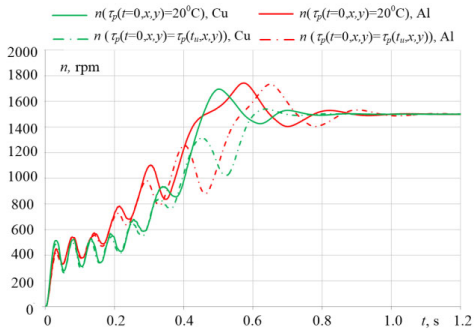

Fig. 9. Comparison of rotor speed time curves for $\tau_p(t = 0, x, y) = 20°C$, $\tau_p(t = 0, x, y) = \tau_u(t_u, x, y)$, $T_L = 19.8$ Nm, $J_i = 0.036$ kg·m^2

of the moment of inertia, regardless of the type of material from which the rotor bars were made of and the initial temperature of the motor, all the start-up processes were successful.

The thermal field distributions obtained for $J_i = 0.036$ kg·m^2 at the end of the starting process ($t = 1.2$ s – electromagnetically steady-state) are shown in Figure 10. They show that higher maximum temperatures are obtained for the motor with the copper rotor bars. Due to the greater moment of inertia and a longer start-up time, they are higher than the maximum values of temperature shown in Figure 7.

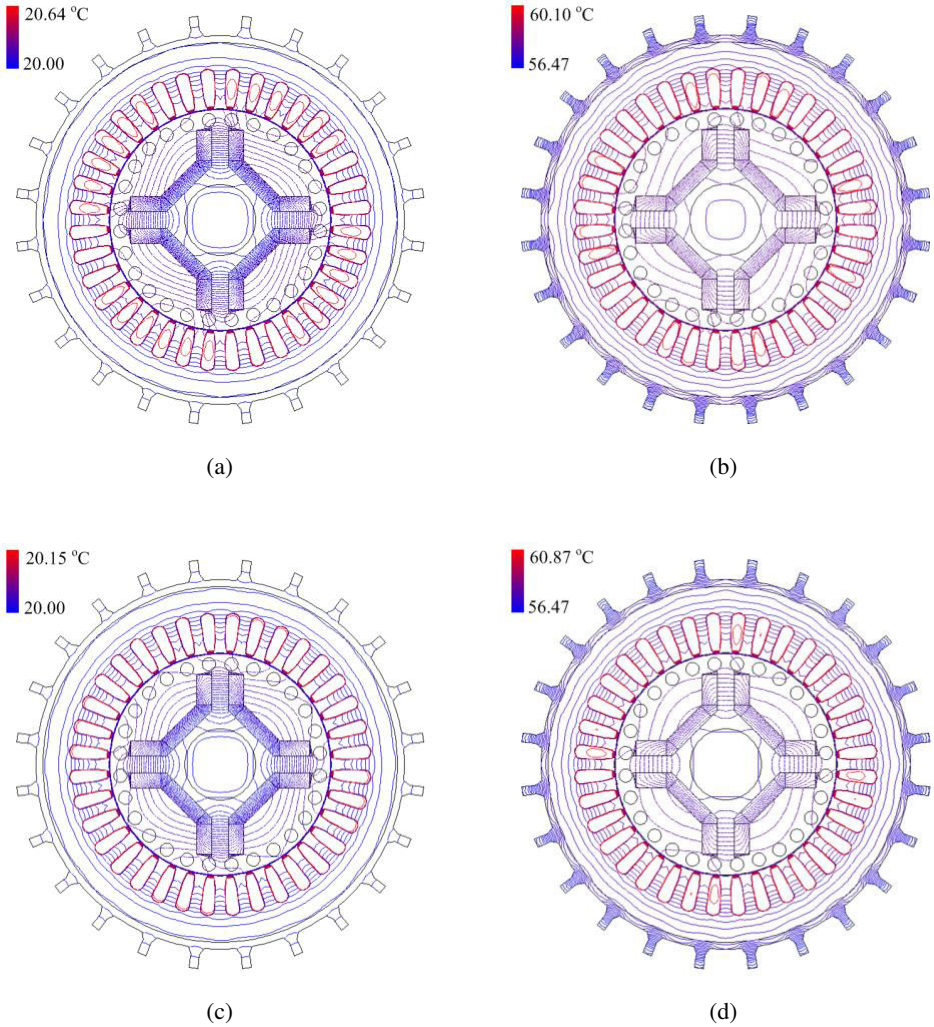

Fig. 10. Thermal field distribution for $t = 1.2$ s in motor with aluminum rotor bars for (a) $\tau_p(t = 0, x, y) = 20°C$; (b) $\tau_p(t = 0, x, y) = \tau_u(t_u, x, y)$ and in motor with copper rotor bars for (c) $\tau_p(t = 0, x, y) = 20°C$; (d) $\tau_p(t = 0, x, y) = \tau_u(t_u, x, y)$, $J_i = 0.036$ kg·m^2, $T_L = 19.8$ Nm

5. Conclusions

The elaborated algorithm and the author's personally developed computer program for the analysis of transient coupled electromagnetic-thermal phenomena in the LSPMSMs were used to analyze a start-up process of motors with aluminum and copper rotor bars. The measurement verification of the temperature distribution in the motor with the aluminum rotor bars aimed at the selection of the heat transfer coefficient κ from the machine surface showed that in a thermal steady-state condition, the difference between the average temperature measured in the stator winding (point A, Figure 2(a)) and the calculated one (point B, Figure 2(a)) is equal to 0.3°C. On the other hand, the difference in the average temperature calculated and measured for the motor with the copper rotor bars (Figure 1(b)) is equal to 0.2°C. The influence of the moment of inertia J_i of the load on the time curves during the start-up process of the considered motors was analyzed. It was found that the starting process of the LSPMSM with the copper rotor bars is possible with a much larger moment of inertia in the movable elements of the system than the motor with the aluminum rotor bars. During the start of the loaded motor with the moment of inertia higher than the nominal moment of inertia of the rotor, a higher maximum temperature is obtained. When analyzing the operating states of the motors, where small temperature changes occur, e.g. starting with a low moment of inertia, it can be assumed that the electrical and thermal properties of the materials do not change. However, with a higher range of temperature changes, for example when the motor is loaded with a high moment of inertia, it is advisable to take into account the influence of temperature on the electrical and thermal properties of materials and, in particular, on the magnetic properties of permanent magnets. Changing the properties of these materials, e.g. changing the demagnetization characteristics of materials the magnets are built of, can have a big impact on the motor's operation. The developed algorithm and software for analyzing coupled phenomena can be used in an LSPMSM design process. The software can be successfully used for the analysis of transients of these types of motors and studies of the influence of temperature increase on the demagnetization of magnets and deterioration of the functional parameters of the motor.

References

[1] Jędryczka C., Knypiński Ł., Demenko A., Sykulski J.K., *Methodology for cage shape optimization of a permanent magnet synchronous motor under line start conditions*, IEEE Transactions on Magnetics, vol. 54, no. 3, pp. 8102304-1–8102304-4 (2018), DOI: 10.1109/TMAG.2017.2764680.

[2] Knypiński Ł., Nowak L., Jędryczka C., *Optimization of the rotor geometry of the line-start permanent magnet synchronous motor by the use of particle swarm optimization*, COMPEL – The International Journal For Computation and Mathematics in Electrical and Electronic Engineering, vol. 34, no. 3, pp. 882–892 (2015).

[3] Łyskawiński W., Jędryczka C., Szeląg W., *Influence of magnet and cage shape on properties of the line start synchronous motor with powder hybrid rotor*, International Symposium on Electrical Machines (SME), on-line: IEEE Xplore, pp. 1–6 (2017), DOI: 10.1109/ISEM.2017.7993556.

[4] Sorgdrager A.J., Wang R.-J., Grobler A.J., *Multiobjective Design of a Line-Start PM MotorUsing the Taguchi Method*, IEEE Transactions on Industry Applications, vol. 54, no. 5, pp. 4167–4176 (2018).

[5] Zawilak J., Gwoździewicz M., *Start-up of large power electric motors with high load torque*, Electrical Review, vol. 95, no. 6, pp. 145–148 (2019), DOI: 10.15199/48.2019.06.27.

[6] Ogbuka C., Nwosu C., Agu M., *Dynamic and steady state performance comparison of line-start permanent magnet synchronous motors with interior and surface rotor magnets*, Archives of Electrical Engineering, vol. 65, no. 1, pp. 105–116 (2016).

[7] Aliabad, A.D., Ghoroghchian F., *Design and analysis of a two-speed line start synchronous motor: Scheme one*, IEEE Trans. Energy Convers., vol. 31, no. 1, pp. 366–372 (2016).

[8] Lee B.H., Jung J.W., Hong J.P., *An improved analysis method of irreversible demagnetization for a single-phase line-start permanent magnet motor*, IEEE Transactions on Magnetics, vol. 54, no. 11, ID: 8206905 (2018).

[9] Ugale R.T., Chaudhari B.N., *Rotor configurations for improved starting and synchronous motor*, IEEE Trans. Ind. Electron., vol. 64, no. 1, pp. 138–148 (2017), DOI:10.1109/TIE.2016.2606587.

[10] Pałka R., Woronowicz K., Kotwas J., Xing W., Chen H., *Influence of different supply modes on the performance of linear induction motors*, Archives of Electrical Engineering, vol. 68, no. 3, pp. 473–483 (2019), DOI: 10.24425/aee.2019.129335.

[11] Knypiński Ł., Jędryczka C., Demenko A. *Influence of the shape of squirrel-cage bars on the dimensions of permanent magnets in an optimized line-start permanent magnet synchronous motor*, COMPEL - The International Journal for Computation and Mathematics in Electrical and Electronic Engineering, vol. 36, no. 1, pp. 298–308 (2017).

[12] Hongbo Q., Yong Z., Kaiqiang H., Cunxiang Y., Ran Y., *The influence of stator winding turns on the steady-state performances of line-start permanent magnet synchronous motors*, Energies, vol. 12, no. 12, pp. 1–15 (2019), DOI: 10.3390/en12122363.

[13] Baranski M., Szelag W., Jedryczka C., *Influence of temperature on partial demagnetization of the permanent magnets during starting process of line start permanent magnet synchronous motor*, International Symposium on Electrical Machines (SME), on-line: IEEE Xplore, p. 6 (2017), DOI: 10.1109/ISEM.2017.7993535.

[14] Ganesan A.U., Chokkalingam L.N., *Review on the evolution of technology advancements and applications of line-start synchronous machines*, IET Electric Power Applications, vol. 13, no. 1, pp. 1–16 (2019).

[15] Xinmai G., Xuefan W., Zhongcao W., *Design and control of high-capacity and low-speed doubly fed start-up permanent magnet synchronous motor*, IET Electric Power Applications, vol. 12, no. 9, pp. 1350–1356 (2018), DOI: 10.1049/iet-epa.2018.5093.

[16] Barański M., Szeląg W., *Finite element analysis of transient electromagnetic-thermal phenomena in a squirrel cage motor working at cryogenic temperature*, IET Science Measurement and Technology, vol. 6, no. 5, pp. 1–7 (2012), DOI: 10.1049/iet-smt.2011.0115.

[17] Demenko A., *Movement simulation in finite element analysis of electric machine dynamics*, IEEE Transactions on Magnetics, vol. 32, no. 3, pp. 1553–1556 (1996).

[18] Baranski M., *FE analysis of coupled electromagnetic-thermal phenomena in the squirrel cage motor working at high ambient temperature*, COMPEL – The International Journal for Computation and Mathematics in Electrical and Electronic Engineering, vol. 38 no. 4, pp. 1120–1132 (2019), DOI: 10.1108/COMPEL-10-2018-0384.

[19] Hameyer K., Driesen J., De Gersem H., Belmans R. *The classification of coupled field problem*, IEEE Transactions on Magnetics, vol. 35, no. 3, pp.1618–1621 (1999).

[20] Driesen J., *Coupled electromagnetic–thermal problems in electrical energy transducers*, PhD Thesis, Faculty of Applied Science, Katholieke Universiteit Leuven, Leuven (2000).